Available online at www.sciencedirect.com
SCIENCE DIRECT®
Journal of Crystal Growth 266 (2004) 264–270
JOURNAL OF CRYSTAL GROWTH
www.elsevier.com/locate/jcrysgro

SP_N-approximations of internal radiation in crystal growth of optical materials

Rainer Backofen, Thomas Bilz, Angel Ribalta, Axel Voigt*

Crystal Growth Group, Research Center caesar, Ludwig-Erhard-Allee 2, D-53175 Bonn, Germany

Abstract

Simplified P_N (SP_N) approximations to the equation of radiative heat transfer are applied to study the effect of internal radiation on the solid/liquid interface in Bridgman growth of semitransparent materials. An adaptive finite element method is derived for SP_1 and SP_2 approximations in combination with phase-change and used to simulate the solidification of a material related to BaF_2.

PACS: 44.40.+a; 44.05.+e; 81.10.Fq

Keywords: A1. Computer simulation; A1. Heat transfer; A1. Radiation; A2. Bridgman technique; B1. Halides

1. Introduction

Theoretical studies of internal radiation in crystal growth of semitransparent materials show that this phenomena can significantly effect the solid/liquid interface, see Refs. [1–5]. Materials of interest are yttrium alumnium garnet YAG, gadolinium gallium garnet GGG, sapphire Al_2O_3 as well as calcium and barium fluoride CaF_2, BaF_2. These crystals are commonly grown from the melt and are semitransparent at the occuring high temperatures during growth. In order to account for internal radiation the radiative heat transfer model which consists of the energy balance equation, in a quasi-stationary approximation

$$-\nabla\cdot k\nabla T+\int_{\nu_1}^{\infty}\int_{S^2}\kappa(I_{\mathrm{B}}-I)\,\mathrm{d}\omega\,\mathrm{d}\nu -\nabla\cdot h\Theta(T-T_{\mathrm{m}})=0 \tag{1.1}$$

and an equation of transfer

$$\forall \nu>\nu_1,\ \omega\in S^2:\omega\cdot\nabla I = -\kappa I+\kappa I_{\mathrm{B}}-\sigma_{\mathrm{s}}I +\frac{\sigma_s}{4\pi}\int_{S^2} I(\omega')\Phi(\omega',\omega)\,\mathrm{d}\omega' \tag{1.2}$$

has to be solved. These equations involve the direction-dependent thermal radiation field, which makes the numerical solution complicated and expensive. Besides the spatial, time and frequency variable, also the directional variable must be included which gives a seven-dimensional phase-space. Therefore sufficiently accurate but less expensive approximations of the radiative transport model are needed. Applied

*Corresponding author. Tel.: +49-228-9656236; fax: 49-228-9656187.
E-mail address: voigt@caesar.de (A. Voigt).

0022-0248/$ - see front matter © 2004 Elsevier B.V. All rights reserved.
doi:10.1016/j.jcrysgro.2004.02.054

Nomenclature

α	hemispherical absorptivity
ε	scaling parameter
ϕ	scalar flux
ϕ_i	scalar flux in $[v_i, v_{i+1}]$
Φ	scattering kernel
h	latent heat per unit area in growth direction
h_0	heat convection coefficient
I	intensity
I_1	integration parameter
I_B	Planck's function
I_B^b	Planck's function at T_b
κ	absorption coefficient
κ_i	absorption coefficient in $[v_i, v_{i+1}]$
κ_{ref}	reference absorption coefficient
k	heat conduction coefficient
l	latent heat
n	outer normal
N	conduction-to-radiation parameter
τ	optical thickness
n_1	refractive index for crucible
n_2	refractive index for crystal/melt
v	frequency
v_1	lower bound for non-opaque spectrum
v_i	bound for frequency band
$r_{1,2,3}$	integration parameter
ρ	hemisherical reflectivity
ρ_s	density
σ_s	scattering coefficient
S^2	unit sphere
Θ	phase function
T	temperature
T_m	melting temperature
T_b	external temperature
v	velocity
x_{ref}	reference length
ψ	test function
ω	direction

approximations to radiative transfer in crystal growth simulation are Rosseland, spherical harmonics (P_N) and discrete ordinates methods. As a method with higher accuracy than simple diffuse approximations mainly P_1 approximations are used for simulating crystal growth processes, see Ref. [5–7].

We propose a simpler SP_N approximation, as an alternative to the P_N equations, which consists of a coupled system of diffusion equations, depending on space, time and frequency, but not direction. For $N > 1$ the number and complexity of the SP_N equations is considerably reduced compared with the P_N equations, leading to only one additional equation for each increment in N and therefore also to much simpler boundary conditions. The SP_N approximation was introduced in the field of nuclear reactor theory Ref. [8]. Due to a lack of theoretical foundation it was not paid much attention to this method until in Refs. [9,10] the SP_N equations and boundary conditions have been derived by an asymptotic and variational analysis. There it was shown that the SP_N equations are higher-order asymptotic solutions of the transport equation in a regime in which diffusion theory is the leading order approximation. The SP_N equations reduce to the P_N equations in planar geometries and especially SP_1 is equal to P_1 in all geometries. Numerical results consistently show that the SP_N approximations can yield more accurate solutions to radiative transport problems than the diffusion approximation with considerably less computational expense than P_N approximations, Refs. [10,11]. Furthermore there it was shown that in situations where the P_1 solution is a good approximation to the radiative heat transfer model, the SP_2 solution is usually even more accurate. The SP_N method was used for example to simulate the annealing in glass manufacturing in Ref. [12] where the obtained results for SP_1 and SP_2 show good agreement with the solution of the full radiative heat transfer model.

We now apply the method to the growth process of semitransparent crystals. An adaptive finite element method is used to study the influence of internal radiation on the solid/liquid interface in Bridgman growth.

2. SP_N approximation

Neglecting scattering effects in the transport equation for the radiative field leads to the SP_N approximation. This allows optically thick regimes, where the absorption coefficient κ is large, to consider in a diffusion-like manner. To obtain a diffusion scaling, the parameter $\varepsilon = 1/\kappa_{\mathrm{ref}} x_{\mathrm{ref}}$ and an appropriate rescaling is introduced, leading to

$$\varepsilon\omega \cdot \nabla I = -\kappa I + \kappa I_{\mathrm{B}} \tag{2.3}$$

or

$$\left(1 + \frac{\varepsilon}{\kappa}\omega \cdot \nabla\right) I = I_{\mathrm{B}}, \tag{2.4}$$

where the same symbols for the rescaled operators are used as before. Applying a Neumann series to formally invert the transport operator leads to

$$\begin{aligned} I &= \left(1 + \frac{\varepsilon}{\kappa}\omega \cdot \nabla\right)^{-1} I_{\mathrm{B}} \\ &= \left(1 - \frac{\varepsilon}{\kappa}\omega \cdot \nabla + \frac{\varepsilon^2}{\kappa^2}(\omega \cdot \nabla)^2 - \frac{\varepsilon^3}{\kappa^3}(\omega \cdot \nabla)^3 \right. \\ &\quad \left. + \frac{\varepsilon^4}{\kappa^4}(\omega \cdot \nabla)^4 + \ldots\right) I_{\mathrm{B}}. \end{aligned}$$

Now integrating over ω, using $\int_{S^2}(\omega \cdot \nabla)^n \mathrm{d}\omega = (1 + (-1)^n)[2\pi/(n+1)]\nabla^n$ and defining the scalar flux

$$\phi = \int_{S^2} I \mathrm{d}\omega$$

led by again formally applying a Neumann series to

$$4\pi I_{\mathrm{B}} = \left(1 - \frac{\varepsilon^2}{3\kappa^2}\nabla^2 - \frac{4\varepsilon^4}{45\kappa^4}\nabla^4 - \frac{44\varepsilon^6}{945\kappa^6}\nabla^6\right)\phi + O(\varepsilon^8).$$

When terms of $O(\varepsilon^2)$, $O(\varepsilon^4)$ or $O(\varepsilon^6)$ are discarded the SP_0, SP_1 or SP_2 approximations are obtained

SP_0

$$\begin{aligned} \kappa\phi &= 4\pi\kappa I_{\mathrm{B}}, \\ &\quad - \nabla \cdot k\nabla T - \int_{\nu_1}^{\infty} \nabla \cdot \frac{1}{3\kappa}\nabla\phi \ \mathrm{d}\nu \\ &\quad - \nabla \cdot h\Theta(T - T_{\mathrm{m}}) = 0, \end{aligned}$$

SP_1

$$\begin{aligned} &- \varepsilon^2 \nabla \cdot \frac{1}{3\kappa}\nabla\phi + \kappa\phi = 4\pi\kappa I_{\mathrm{B}}, \\ &-\nabla \cdot k\nabla T - \int_{\nu_1}^{\infty} \nabla \cdot \frac{1}{3\kappa}\nabla\phi \ \mathrm{d}\nu - \nabla \cdot h\Theta(T - T_{\mathrm{m}}) = 0 \end{aligned}$$

SP_2

$$\begin{aligned} &- \varepsilon^2 \nabla \cdot \frac{1}{3\kappa}\nabla\left(\phi + \frac{4}{5}(\phi - 4\pi I_{\mathrm{B}})\right) + \kappa\phi = 4\pi\kappa I_{\mathrm{B}}, \\ &- \nabla \cdot k\nabla T - \int_{\nu_1}^{\infty} \nabla \cdot \frac{1}{3\kappa}\nabla\left(\phi + \frac{4}{5}(\phi - 4\pi I_{\mathrm{B}})\right)\mathrm{d}\nu \\ &\quad - \nabla \cdot h\Theta(T - T_{\mathrm{m}}) = 0. \end{aligned}$$

Of course also higher approximations can be derived by this method. Even if the formal derivation is obtained for constant parameters κ the resulting equations are assumed to be valid also for nonconstant parameters. The SP_0 approximation reduced to an equation for the temperature T alone, and is the conventional Rosseland approximation.

$$\begin{aligned} &- \nabla \cdot k\nabla T - \nabla \cdot \left(\frac{4\pi}{3}\int_{\nu_1}^{\infty} \bar{\kappa}\frac{\partial I_{\mathrm{B}}}{\partial T} \ \mathrm{d}\nu\right)\nabla T \\ &\quad - \nabla \cdot h\Theta(T - T_{\mathrm{m}}) = 0. \end{aligned} \tag{2.5}$$

Despite the different derivation of SP_1 and P_1 approximation, by comparison of the partial differential equations, it can be easily shown that P_1 is equivalent to SP_1 in all cases. In a plan parallel situation P_N collapses to the SP_N equation for all N.

Starting from semitransparent boundary conditions for the radiative heat transfer model similar to the P_N approximations Marshak's condition, see Ref. [13], is used in order to derive suitable boundary conditions for the SP_N approximations, which lead to

$$kn \cdot \nabla T = h_0(T_{\mathrm{b}} - T) + \alpha\pi\left(\frac{n_1}{n_2}\right)^2 \int_0^{\nu_1} I_{\mathrm{B}}^{\mathrm{b}} - I_{\mathrm{B}} \ \mathrm{d}\nu \tag{2.6}$$

for temperature T and

$$\begin{aligned} &\forall \nu > \nu_1\colon (1 - 2r_1)\phi + \varepsilon(1 + 3r_2)\frac{2}{3\kappa}n \cdot \nabla\phi \\ &\qquad = 4\pi(1 - 2r_1)I_{\mathrm{B}}^{\mathrm{b}} \end{aligned} \tag{2.7}$$

$$\begin{aligned} &\forall \nu > \nu_1\colon (1 - 2r_1)\phi \\ &\quad + \varepsilon(1 + 3r_2)\ \frac{2}{3\kappa}n \cdot \nabla\left(\phi + \frac{4}{5}(\phi - 4\pi I_{\mathrm{B}})\right) \\ &\quad + (1 - 4(3r_3 - r_1))\ \frac{1}{2}\ (\phi - 4\pi I_{\mathrm{B}}) \\ &\qquad = 4\pi(1 - 2r_1)I_{\mathrm{B}}^{\mathrm{b}} \end{aligned} \tag{2.8}$$

for the scalar flux ϕ for SP_1 and SP_2, respectively, with

$$r_1 = \int_0^1 \mu\rho(-\mu)\mathrm{d}\mu, \quad r_2 = \int_0^1 \mu^2\rho(-\mu)\mathrm{d}\mu \quad \text{and}$$
$$r_3 = \int_0^1 \mu^3\rho(-\mu)\mathrm{d}\mu.$$

A detailed derivation of the boundary conditions may be found in Ref. [12].

3. Finite element discretisation

The phase-change is considered similar as in Ref. [14]. The latent heat per unit area in growth direction is defined as $h = \rho_s l v$. The phase-function Θ is regularized by a small parameter δ and is given by

$$\Theta(T) = \begin{cases} -1: & T < T_m - \delta, \\ -1 + \left(1 + \dfrac{T - T_m}{\delta}\right): & T_m - \delta < T < T_m, \\ 1 - \left(1 - \dfrac{T - T_m}{\delta}\right): & T_m < T < T_m + \delta, \\ 1: & T > T_m + \delta. \end{cases}$$

The phase-boundary is defined by the isotherm at T_m. Before deriving a weak formulation we use the chain-rule to transfer $-\nabla \cdot h\Theta(T - T_m)$ to $-\Theta'(T - T_m)h \cdot \nabla T$ and approximate the integrals over the frequency by a sum over frequency bands $[v_i, v_{i+1}]$ in which the involved parameters are assumed to be constant. By defining $\phi_i = \int_{v_i}^{v_{i+1}} \phi \, \mathrm{d}v$, multiplying with a test function ψ and integrating by parts a weak formulation is obtained for the SP_0, SP_1 and SP_2 approximations, which is only stated here for SP_1

$$\varepsilon^2 \frac{1}{3\kappa_i} \int_\Omega \nabla\phi_i \cdot \nabla\psi - \frac{2\varepsilon}{3\kappa_i(1 + 3r_2)} \int_{\partial\Omega} \left(\int_{v_i}^{v_{i+1}} I_1 \, \mathrm{d}v \right) \psi + \frac{\varepsilon(1 - 2r_1)}{6\kappa_i(1 + 3r_2)} \int_{\partial\Omega} \phi_i\psi + \kappa_i \int_\Omega \phi_i\psi = 4\pi\kappa_i \int_\Omega \left(\int_{v_i}^{v_{i+1}} I_B \mathrm{d}v \right) \psi, \quad i = 1, 2, \ldots$$

$$\int_\Omega k\nabla T \cdot \nabla\psi - \int_{\partial\Omega} h_0(T_b - T)\psi - \int_{\partial\Omega} \left(\alpha\pi \left(\frac{n_1}{n_2}\right)^2 \int_0^{v_1} I_B^b - I_B \, \mathrm{d}v \right) \psi + \sum_i \left(\frac{1}{3\kappa_i} \int_\Omega \nabla\phi_i \cdot \nabla\psi - \frac{2}{\varepsilon(1 + 3r_2)} \times \int_{\partial\Omega} \left(\int_{v_i}^{v_{i+1}} I_1 \, \mathrm{d}v \right) \psi + \frac{1 - 2r_1}{2\varepsilon(1 + 3r_2)} \int_{\partial\Omega} \phi_i\psi \right) - \int_\Omega \Theta'(T - T_m)h \cdot \nabla T\psi = 0.$$

This system is now discretized by linear finite elements and iteratively solved by a Newton method. In order to account for the high spacial resolution needed at the phase-boundary as well as at the developing boundary layers, due to the radiative effects an error indicator for temperature is used for local mesh refinement. We use an error estimate as in Ref. [15], taking account of both the phase change and the radiative effects.

4. Results and discussion

In this section, the numerical results obtained from the SP_1 and SP_2 approximations are considered. In order to test the numerical algorithms we start with a one-dimensional problem without phase-change. A region of length L with a single semitransparent material is confined by perfectly black surfaces. The temperatures at the surfaces are fixed at $T_1 = T(x = 0) = 1000\,\mathrm{K}$ and $T_2 = T(x = L) = 500\,\mathrm{K}$. In this slab geometry the equation for radiative heat transport reduces to a simple integral equation [13]:

$$q_{rad}(x) = 2\pi I_B^1 E_3(\kappa x) - 2\pi I_B^2 E_3(\kappa(L - x)) + 2\pi \int_0^x I_B(x')E_2(\kappa(x - x'))\mathrm{d}x' - 2\pi \int_x^L I_B(x')E_2(\kappa(x' - x))\mathrm{d}x', \qquad (4.9)$$

where $E_n(x) = \int_0^\infty \exp(-xt)dt/t^n$ is the exponential integral of order n. Combined with Eq. (1.1), the heat transport due to radiation and diffusion in one dimension may be easily solved numerically Ref. [13]. For discussion the two governing

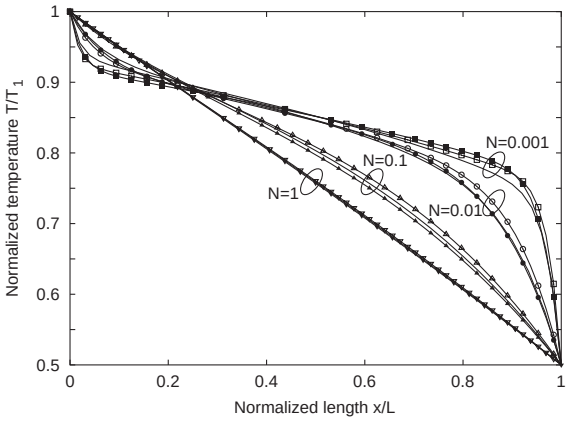

Fig. 1. Normalized temperature in one-dimensional slab geometry. Solid lines indicate the solution obtained by solving the exact heat transport equation. Lines with open symbols correspond to results from SP_1 approximation of heat transfer. Lines with closed symbols correspond to SP_2 approximation.

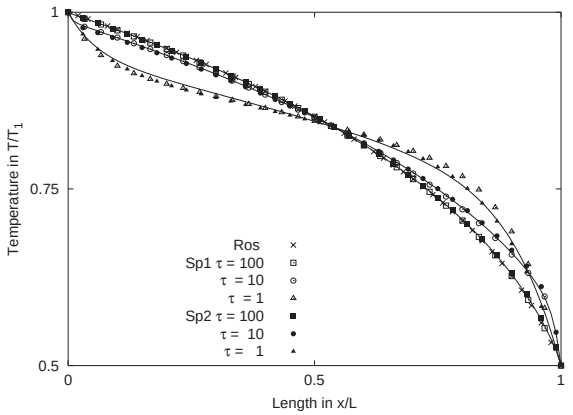

Fig. 2. Nondimensional temperature distribution for different optical thickness τ. Solid lines are obtained by the exact heat transport equation, crosses corresponds to solution of the Rosseland model and open symbols are calculated by SP_1 approximation.

dimensionless numbers are introduced: the optical thickness $\tau = \kappa x'$ and the conduction-to-radiation parameter $N = (k\kappa)/(4\sigma n^2 T'^3)$ where primed values are typical length scales, x', and Temperatures, T'. Fig. 1 shows the solution of the exact radiative transfer equation for 4 different conduction-to-radiation parameters N in comparison with the SP_1 and SP_2 results. A single frequency band was used. With decreasing N, the influence of radiation increases and the temperature profile changes from linear to a behaviour with rapid changes at the boundaries.The limit $N \to 0$ would lead to a discontinuity at the boundaries. The temperature profile predicted by the SP_N-models quite good agrees with the results obtained by solving the exact heat transfer equation. But there is no clear evidence, that SP_2 is in general more or less accurate than SP_1. The SP_N equations are derived for optical thick materials. So, to check for validity of the approximation calculations are performed for a fixed $N = 0.01$ and varying τ, Fig. 2. In this case the temperature distribution obtained by the Rosseland approximation is independent on τ. The Rosseland approximation perfectly agrees for $\tau \geqslant 100$. For smaller τ the exact temperature distribution begins to differ from the Rosseland solution. In this simple case the SP_N - models predict the temperature distribution quite good for all τ. This is mainly due to the simple boundary conditions.

Semitransparent or flux boundary conditions are likely to change the situation for small τ.

The algorithm is now applied to a three-dimensional situation with phase-change. Therefore a vertical Bridgman process for a semitransparent material related to BaF_2 is considered. An ampoule of diameter 11mm and length 70 mm is chosen as the computational domain. The temperature at the surface is fixed and increases linearly in height. The gradient of temperature at the surfaces is 15 K/cm according to a global simulation of a Bridgman furnace used in Ref. [16]. The pulling velocity is $v = 3$ mm/h. Together with a density of $\rho = 4830$ Kg/m^3 and a latent heat of $l = 3.8 \times 10^5$J/Kg these lead to a latent heat per unit area in growth direction of $h = 1529.5$ W/m^2. For the solid phase of BaF_2 a heat conduction coefficient of $k_s = 2.4$ W/mK is chosen, whereas for the liquid phase $k_m = 0.24$W/mK is applied. All these parameters are taken from [16]. Here N and τ are derived according to $T_{melt} = 1628$K and the crucible diameter.

The influence of internal radiation on the deflection of the solid/liquid interface is now studied. Fig. 3 shows the final adaptive grid obtained without radiative effects, with SP_1 and

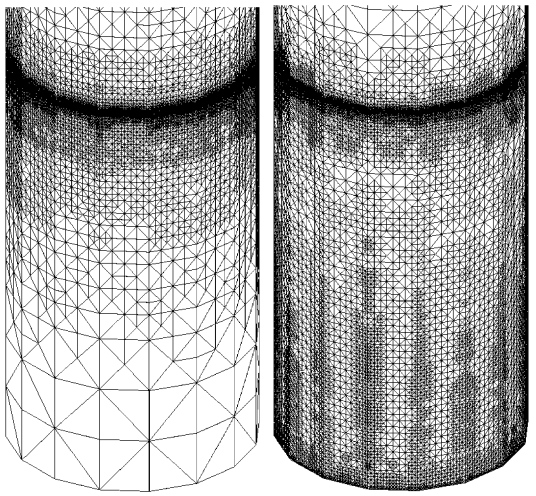

Fig. 3. Adaptively refined grid at the solid/liquid interface and radiative boundary layers. (a) without radiation, (b) SP_1, the grid obtained for SP_2 on this level of detail coincides with the one for SP_1.

SP_2 approximations. All grids are refined until the temperature distribution is independent of the grid, leading to a strong refinement at the solid–liquid interface. The grids obtained with SP_1 and SP_2 approximations are in additions refined at the boundary layers on the top and bottom of the ampoule. In the used set up assuming a fully transparent material or a opaque material gives the same temperature distribution inside the cylinder. In both cases the thermal field inside the cylinder is completely defined by diffusion only:

- In the opaque case ($N \to \infty$) the heat transfer by conduction just governs the heat transfer by radiation.
- In the transparent case ($\tau \to 0$) the radiation just passes through the material without coupling into the thermal field.

But the total heat flux through the cylinder is surely different for transparent and opaque material. Due to the different conductivities in melt and crystal the phase boundary is predicted to bend towards the melt. The latent heat reduce this effect. Now for semitransparent material the radiative heat transport becomes important. As

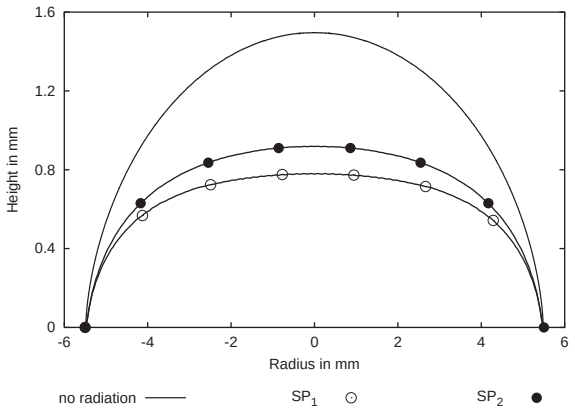

Fig. 4. Phase boundary in a cut through the center of the ampoule for the three cases: without radiation, SP_1 and SP_2. The optical thickness is $\tau = 1$.

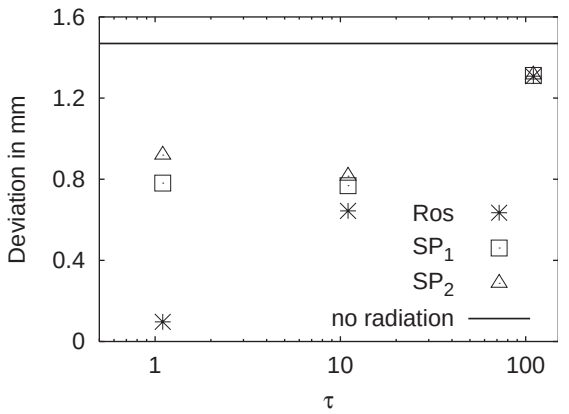

Fig. 5. Bending of phase boundary in the center of the ampoule over optical thickness for the four cases: without radiation, Rosseland (Ros), SP_1 and SP_2.

the absorption is constant in the material the ratio of the effective conductivity in crystal and melt decreases. Therefore the phase boundary flattens. All treated models qualitatively show this behavior. Fig. 4 shows the phase-boundary along a cut through the center of the ampoule for the opaque or transparent case and the semitransparent SP_1 and SP_2 approximations. The obtained results for SP_1 and SP_2 both qualitatively show the described flattening of the phase-boundary. But quantitative result whether SP_1 or SP_2 gives higher accuracy can not be given. In Fig. 5 the bending of the phase boundary in the center is shown for varying optical

thickness. Comparing the different approximations we conclude: For $\tau = 100$ the SP_0, SP_1 and SP_2 solutions coincide, which agrees with the assumption that the Rosseland approximations is valid for such an optical thickness. For $\tau = 10$ the SP_1 and SP_2 approximation still show the same behaviour, but the SP_0 approximation deviates from this shape and predicts a phase boundary which is to low. By further decreasing τ the SP_0 approximation is not valid anymore and only included here for completeness. For $\tau = 1$ the SP_1 and SP_2 approximation deviate from each other.

5. Conclusion

Modeling three-dimensional radiative heat transfer in semitransparent media is still a challenging task in crystal growth. Especially for process optimization efficient and sufficiently accurate algorithms are needed. Furthermore, the mostly used and mature techniques for solving heat transport phenomena in crystal growth are solvers for the underlying partial differential equations. So, in order to extend already used programs and tools to include effects due to internal radiation, numerical models based on partial differential equations are favorable. The SP_N approximations are a series of high order derivations of the scalar flux ϕ in space and may be reformulated as a set of elliptic partial differential equations.

In the optical thick regime the SP_N approximation is a good candidate to extend modeling of radiative effects beyond Rosseland (SP_0) approximation. The SP_1 approximation, which is equivalent to the P_1 approximation already shown reasonable results for wide range of semitransparent materials. Even order SP_N approximation has to be used with care. The strong connection between SP_N and P_N approximation may lead to inferior results of even order compared to a lower odd order approximation. In Ref. [11] however it is mentioned that in situations, where SP_1 is already a good approximation SP_2 improves the results. In modeling of glass cooling processing higher order SP_N approximation already proofed their applicability. But for crystal growth, the range of applicability still has to be determined in detail.

Acknowledgement

This work was partially supported by BMBF through 03HOM3CA and 03N1038.

References

[1] S. Brandon, J.J. Derby, J. Crystal Growth 121 (1992) 473.
[2] S. Brandon, J.J. Derby, J. Crystal Growth 110 (1991) 481.
[3] T. Tsukada, K. Kakinoki, M. Hozawa, N. Imaishi, Int. J. Heat Mass Transfer 38 (1995) 2707.
[4] M. Kobatashi, T. Hagino, T. Tsukada, M. Hozawa, J. Crystal Growth 235 (2002) 258.
[5] C.W. Lan, C.Y. Tu, Y.F. Lee, Int. J. Heat Mass Transfer 46 (2003) 1629.
[6] H. Matsushima, R. Viskata, Int. J. Heat Mass Transfer 33 (1990) 1957.
[7] J.J. Derby, S. Brandon, A.G. Salinger, Int. J. Heat Mass Transfer 41 (1998) 1405.
[8] E.M. Gelbard, Technical Report WAPD-T-1182, Bettis Atomic Power Laboratory, 1961.
[9] E. Larsen, J.E. Morel, J.M. McGhee, Nucl. Sci. Eng. 123 (1996) 328.
[10] P.S. Brantley, E. Larsen, Nucl. Sci. Eng. 135 (2000) 199.
[11] D.I. Tomasevic, E.W. Larsen, Nucl. Sci. Eng. 122 (1996) 309.
[12] E. Larsen, G. Thömmes, A. Klar, M. Seaid, T. Götz, J. Comput. Phys. 183 (2002) 652.
[13] M.F. Modest, Radiative Heat Transfer, McGraw-Hill, New York, 1993.
[14] M. Kurz, A. Pusztai, G. Müller, J. Crystal Growth 198–199 (1999) 101.
[15] R. Verfürth, A Review of A Posteriori Error Estimation and Adaptive Mesh–Refinement Techniques, Wiley and Teubner, New York, 1996.
[16] F. Barvinschi, O. Bunoiu, I. Nicoara, J.T. Santailler, T. Duffar, J. Crystal Growth 237–239 (2002) 1762.